Ocean Engineering 272 (2023) 113827

Contents lists available at ScienceDirect

Ocean Engineering

journal homepage: www.elsevier.com/locate/oceaneng

Simulation of mooring Lines in complex bathymetries using a finite element method

Paula Desiré [a], Álvaro Rodríguez-Luis [b], Raúl Guanche [b,*]

[a] Universidad de Cantabria, Av. de los Castros, 39005, Santander, Spain
[b] Environmental Hydraulics Institute, Universidad de Cantabria, Avda. Isabel Torres, 15, Parque Científico y Tecnológico de Cantabria, 39011, Santander, Spain

ARTICLE INFO

Keywords:
Complex bathymetry
Projection algorithm
Mooring lines
Numerical model
Finite element method

ABSTRACT

This paper presents a novel method for the modeling of the seabed interaction of mooring lines in complex bathymetries, known as "continuous projection method". This method is able to calculate ground normal and friction forces for any seafloor surface. This provides an improvement in the mooring systems simulation, as it captures additional non-linearities on the mooring line performance due to seabed interaction.

The method is based on constructing a triangulation for the seabed and projecting mooring line nodes by using the vertex normal vectors of each triangle, ensuring the continuity of the projection. For the sake of the computational cost reduction, the line nodes are first projected into the closest triangles. Also, whenever the floor is flat, inclined or horizontal, a point-to-plane projection expression is used instead. The projection method described has been implemented to a finite element model. The initial condition problem was solved with a static approach, based on finding the static equilibrium with Newton–Armijo algorithm. This improves other static approaches which use the catenary equation, and that are only valid for a flat seabed.

The model was successfully verified against the analytical solution of an inextensible catenary line in a slope. Furthermore, the simulation results were validated against experimental scale tests on a single chain mooring line with three different seafloor structures: one flat floor and two different sloped steps. For each of them, static and dynamic regular tests were performed. Moreover, high and low frequency fairlead movements were imposed in the dynamic tests, aiming to validate the model both in cases with and without snapping loads. Overall, the obtained results were coherent and allow to validate the accuracy of the proposed model. Finally, a mooring line over an irregular seabed surface was studied, comparing the results obtained by directly applying the developed method for complex bathymetries, by interpolating the surface by an inclined plane and using the constructed projection algorithm for that case or, by last, approximating by a flat seafloor. The comparison of the results among the different approaches illustrates the importance of considering the seabed slope and irregularities for the fairlead tension prediction. Also, this flat seafloor was evaluated with two different projection methods: the one specific for horizontal seafloors and the one developed for general seabed surfaces. This allows to compare the computational time required in both of them.

1. Introduction

Wave and wind power are called to become a renewable and clean energy source. In fact they are currently a global interest topic. Both can be highly exploited in deep water areas by the installation of floating structures secured by mooring systems. Therefore, an anomalous performance of the mooring system could result in a damage or even a loss of the devices. Mooring lines are anchored to the seabed and connected to a point close to the sea surface called fairlead, located in a floating platform. These lines need to withstand high peak loads that mostly occur when the mooring line slacks and then is retightened. This behavior is commonly referred as snap-slack or snap loads. Studies in Norway (Rolfsen et al., 2013) showed that dynamic snap loads caused an excess load on mooring lines, producing one of the most common causes of failure of mooring systems. In addition, snap loads also increase the fatigue damage of the line. Accurately predicting the complete dynamics of the mooring can avoid possible failures and will result in cost saving, and numerical simulations provide a useful tool to develop this prediction.

A wide range of the numerical simulations developed for moorings are based on the finite element method. Aamo and Fossen (2000) worked with linear finite elements, and Montano et al. (2007) implemented Continuous Galerkin method in their work. In addition, Palm

* Corresponding author.
E-mail address: guancher@unican.es (R. Guanche).

https://doi.org/10.1016/j.oceaneng.2023.113827
Received 8 June 2022; Received in revised form 12 September 2022; Accepted 27 January 2023
Available online 8 February 2023

et al. (2017) have already used Discontinuous Galerkin obtaining accurate results. Lumped mass models (Hall and Goupee, 2015; Azcona et al., 2017) are also a common approach in mooring line simulations. The presented work is based on the previous work developed by Rodríguez et al. (2020), a numerical method which simulates the dynamics of a mooring system using finite element method (FEM) first order elements and Continuous Galerkin. In the cited model, a static approach based on the catenary equations is used in order to solve FEM's initial condition problem. For the temporal simulation, a dynamic approach which emphasizes the importance of different non-linear forces such as tension, internal damping or friction is preferred.

Gobat and Grosenbaugh (2001) concluded in their work that studying with precision the seabed interaction is crucial, as it generates snap loads when the contact point speed exceeds the transverse wave speed of the mooring. Feng et al. (2016) have previously studied that the seafloor surface significantly influences the hydrodynamic characteristics of the floating body. In addition, there are certain external forces to which the mooring line is subjected that strongly depend on the seabed surface such as normal ground or friction forces, whose importance for developing accurate models has already been discussed by Devries and Hall (2018).

However, the seabed surface is usually approached by a flat plane, introducing an error for not only snap tensions but also for line positioning. Complex bathymetries can appear at any seafloor depth, but there are some points in which its relevance increases such as the continental shelf, as it leads to a strong change in bathymetry. It also produces problems in certain locations in which the seabed surface presents significant irregularities such as in the Canary Islands, a target site where the absence of continental shelf leads to large seabed slopes.

A two dimensional static numerical model of a mooring line in a slope has already been developed (Feng et al., 2020). In addition, Thomsen et al. (2017) cites three different software able to simulate mooring lines in seabeds modeled as horizontal, sloping or with a three dimensional bathymetry: *OrcaFlex, Flexcom* and *ProteusDS*. They are also equipped with friction models that consider the seabed structure. In the OrcaFlex user guide (OrcaFlex, 1987-2022) it is explained that the seabed coordinates are used to construct a triangulation which is interpolated by either a linear or a cubic polynomial method. The (Flexcom, 2021), has also utilized the cubic interpolation method of the triangulation. software (ProteusDS, 2018) uses a mesh discretizied into squares describing the seabed equipped with polygonal normals able to model ground normal and friction forces. Nevertheless, none of the above methods are described in detail in the scientific community, leaving a gap in literature that this paper tries to fill.

OrcaFlex was used by Jaiswal et al. (2016) in an extensive study which showed significant differences in line tensions between two approaches: considering a complete description of the seabed or approximating it by constant slope planes. In their work, it was concluded that it was specially important to predict with precision the touchdown point location, as line stiffness depends on the weight of the mooring part which goes from the fairlead to the touchdown point: the suspended weight. The location of this point can be radically different if the seabed is modeled by any approximation instead of considering the true representation.

The presented work is focused on developing a new methodology in the three-dimensional simulation of a mooring line laying on any irregular surface seabed. The proposed method is based in a state of the art continuous projection method Orazi and Reggiani (2020), that can be applied to calculate the mooring line friction and normal forces, achieving realistic results in the mooring line positioning as well as in its tensions. The constructed projection algorithm is applicable for both dynamic and static approaches, providing a reliable simulation. In addition, in order to reduce computational cost, the projection algorithm varies when the seabed surface is flat, forms an inclined plane or is a complex bathymetry.

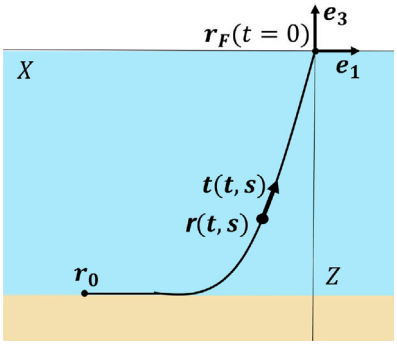

Fig. 1. Graphical description of the system of reference used. r_0 is the anchor position while $r_F(t=0)$ corresponds to fairlead initial position.

The paper is organized as follows: in Section 2, a description of the numerical model used to simulate the mooring line is exposed, followed by the development of the continuous projection method and its application to friction and ground normal forces. Then, in Section 3 a specific situation of the mooring line configuration described by an analytical solution was compared with the numerical obtained results by simulating it, verifying the developed method. Section 4 provides an experimental validation of the model with different seabeds in a quasistatic performance, without snapping loads, as well as of the model in a dynamic performance, with the appearance of snapping loads. Finally, in Section 5 an irregular seabed surface is studied by three different methods whose results were compared: directly applying the developed projection algorithm for complex bathymetries, approximating it to an inclined plane and using the projection algorithm version for these seabed surfaces and approximating it by a flat surface. The work ends with several conclusions explained in Section 6.

2. Model description

This section starts with a brief description of the numerical method in which the simulation of mooring lines developed by the Environmental Hydraulics Institute is based. Later, the novel part is presented. It describes a projection method that can be applied to evaluate the interaction between the mooring line and any seabed, something that the simulation could not do before. This method operates differently depending on whether the seafloor surface is horizontal, inclined plane or irregular. Then, the models used to evaluate friction and ground normal forces are also detailed, as well as some problems that have to be taken into account when a seafloor with irregular surface is introduced.

2.1. Numerical solution of the mooring line dynamics

In this subsection, the mooring line dynamics model and equations are introduced, as well as the finite element method used to solve the arised partial differential equation.

The frame used in this work has its origin of coordinates in the fairlead's projection in the sea surface. The sea surface level corresponds to z = 0, with e_3 pointing opposite to the seabed. Hence, the mooring line z-position is generally negative. The x-axis is parallel to the direction of the vector that joins the fairlead with the anchor, taking negative values as it advances along the mooring line. On the other hand, the y-axis is perpendicular to the ones previously defined. The mentioned graphical frame description can be seen in Fig. 1.

2.1.1. Formulation of the problem

If flexion and torsion effects are ignored, mooring lines dynamics can be modeled by Newton's equation expressed per unit of length. The expression is described in Aamo and Fossen (2000):

$$\gamma_0 \frac{\partial^2 \boldsymbol{r}(t,s)}{\partial t^2} = \frac{\partial}{\partial s}(T(t,s)\boldsymbol{t}(t,s)) + \boldsymbol{f}(t,s)(1+e(t,s)) \tag{1}$$

where γ_0 is the mooring line mass per meter, $s \in [0, L]$ is the arc length parameter, being L the mooring line length; t is the time variable and t_0 is the initial time, $\boldsymbol{r} : [t_0, \infty) \times [0, L] \rightarrow \mathbb{R}^3$ is the position of the mooring line, $T : [t_0, \infty) \times [0, L] \rightarrow \mathbb{R}$ is the mooring tension, $\boldsymbol{t} : [t_0, \infty) \times [0, L] \rightarrow \mathbb{R}^3$ is the unitary tangential vector to the mooring line, $\boldsymbol{f} : [t_0, \infty) \times [0, L] \rightarrow \mathbb{R}^3$ is the external forces vector and $e : [t_0, \infty) \times [0, L] \rightarrow \mathbb{R}$ is the strain of the mooring.

The tension T was modeled by adding a damping coefficient to Hook's law, as it is described by Rodríguez et al. (2020):

$$T = EA(e + \beta \frac{\partial e}{\partial t}) \tag{2}$$

where EA is line's Young's Module multiplied by line's section and β is the internal damping coefficient.

The mooring is subjected to several external forces. Their expressions, based on Palm et al. (2013) description, are the following:

$$\boldsymbol{f} = \boldsymbol{f_{hg}} + \boldsymbol{f_{dn}} + \boldsymbol{f_{dt}} + \boldsymbol{f_{mn}} + \boldsymbol{f_N} + \boldsymbol{f_f} \tag{3}$$

- $\boldsymbol{f_{hg}} = \gamma_0 \frac{\rho_c - \rho_w}{(1+e)\rho_c} \boldsymbol{g}$ is the buoyancy force. ρ_W and ρ_c are the water and mooring line densities per unit of length respectively.
- $\boldsymbol{f_{dn}} = -\frac{1}{2} C_{Dn} d \rho_W |\boldsymbol{v_n}| \boldsymbol{v_n}$ is the hydrodynamic normal drag force. C_{Dn} is the normal drag coefficient, d is the mooring line diameter and $\boldsymbol{v_n}$ the normal velocity.
- $\boldsymbol{f_{dt}} = -\frac{1}{2} C_{Dt} d \rho_W |\boldsymbol{v_t}| \boldsymbol{v_t}$ is the hydrodynamic tangential drag force. C_{Dt} is the tangential drag coefficient and $\boldsymbol{v_t}$ the tangential velocity ($\dot{\boldsymbol{r}}$).
- $\boldsymbol{f_{mn}} = -\frac{\pi d^2}{4} \rho_W C_{MN} \boldsymbol{a_n}$ is the normal added mass force. C_{MN} is the added mass coefficient and $\boldsymbol{a_n}$ the normal acceleration.
- $\boldsymbol{f_n}$ is the ground normal force, described in Eq. (11).
- $\boldsymbol{f_f}$ is the friction force. Its implementation will be shown in Eq. (12).

The problem is fixed in space to Dirichlet boundary conditions. The restrictions are given by the position of the anchor and the fairlead: the anchor is fixed to a point $\boldsymbol{r_0}$ contained in $\mathbb{R}^3$ and the fairlead position is described by a vector $\boldsymbol{r_F} : [t_0, \infty) \rightarrow \mathbb{R}^3$:

$$\boldsymbol{r}(t,0) = \boldsymbol{r_0} \; ; \; \boldsymbol{r}(t,L) = \boldsymbol{r_F}(t) \tag{4}$$

After the application of the finite element method discretization to the arc length parameter in Eq. (1), a time differential equation is obtained, which can be modeled as an initial value problem. Its solution will be discussed in Section 2.3.

2.1.2. Numerical solution of the PDE

Eq. (1) is non-linear, and can be expressed as the following second-order partial differential equation (PDE):

$$\ddot{\boldsymbol{r}} = \Phi(\dot{\boldsymbol{r}}, \boldsymbol{r}, t) \tag{5}$$

The first step to solve this equation is to develop a spatial discretization of the mooring line and using a Galerkin continuous based first order finite element method, as it was done by Aamo and Fossen (2000). The mooring line is divided into N nodes, getting $\mathbf{r}(t,s) = (\boldsymbol{r_0}, \boldsymbol{r_1}, \dots \boldsymbol{r_{N-1}})$. Each mooring line node position is a three dimensional vector with the point coordinates. The spatial boundary conditions must be imposed in this step, being $\boldsymbol{r_{N-1}}$ the position of the fairlead and $\boldsymbol{r_0}$ the position of the fixed anchor.

Following the method proposed by Aamo and Fossen (2000), a linear system of ordinary differential equations (ODE system) is generated. Its solution provides the accelerations ($\dot{\boldsymbol{r}}$) in each mooring line node. In order to temporarily integrate and later solve the ODE system subjected to the initial condition, the second order ODE is reduced to a first order system and finally, a second order implicit backward differential method (Bonaventura and Gómez, 2021), commonly referred as BDF2, is used.

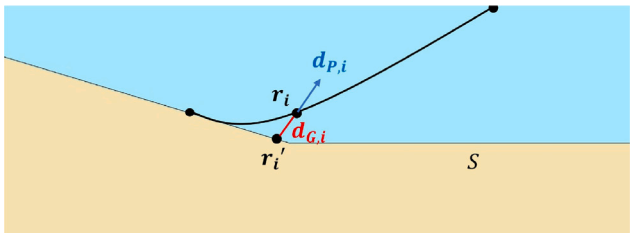

Fig. 2. For a certain mooring line node i with a vector position of $\boldsymbol{r_i}$ and a seabed surface S, the terms $d_{G,i}$ and $\boldsymbol{d_{P,i}}$ have been represented, as well as its projection into the seabed surface, $\boldsymbol{r_i'}$.

2.2. Projection algorithm

The aim of this work is to model the interaction between the mooring line and the seabed, considering all the bathymetry shape complexity. Therefore, there is a great interest in calculating ground normal and friction forces. However, in order to evaluate these forces in a variable seafloor surface, a projection algorithm must be developed.

2.2.1. Formulation of the terms

The calculation of normal and friction forces lays on certain terms which depend on the seabed surface, as it will be presented in Eq. (11) and Eq. (12) respectively.

Let S be the irregular seabed surface. As it was defined above, $\{\boldsymbol{r_i}\}_{i=0}^{N-1}$ is the position of a mooring line node i. Furthermore, $\boldsymbol{r_i'}$ is the closest point to $\boldsymbol{r_i}$ contained in the surface S. That is, each $\boldsymbol{r_i'} \in S$ satisfies that $\forall \boldsymbol{r_G} \in S, \|\boldsymbol{r_i} - \boldsymbol{r_i'}\| \leq \|\boldsymbol{r_i} - \boldsymbol{r_G}\|$. Therefore, $\boldsymbol{r_i'}$ is the projection of $\boldsymbol{r_i}$ in the seabed surface S and, at this point, the unitary normal vector to the seabed surface pointing outwards, is denoted as $\boldsymbol{n_{S,i}}$. In non-convex surfaces, it could be the case that the projection point was not unique, but this problem is already considered in the projection algorithm introduced in Section 2.2.2.2.

It is also interesting to describe the direction of projection, a unitary vector defined as follows:

$$\boldsymbol{d_{P,i}} = \frac{\boldsymbol{r_i} - \boldsymbol{r_i'}}{\|\boldsymbol{r_i} - \boldsymbol{r_i'}\|} \tag{6}$$

The direction of projection should vary in a continuous form between the mooring line nodes in order to avoid computational problems when the jacobian used in the temporal simulation is calculated. Finally, $d_{G,i}$ is defined as the penetration depth of the line node i in the seabed surface S. It is positive when the line node is over the seabed and negative when it is buried into it. In other words:

$$d_{G,i} = (\boldsymbol{r_i} - \boldsymbol{r_i'}) \cdot \boldsymbol{n_{S,i}} \tag{7}$$

It is important to notice the difference between both terms: the $\boldsymbol{d_{P,i}}$ is a three dimensional vector while $d_{G,i}$ is a scalar. A graphical example is introduced in Fig. 2. $d_{G,i}$ will be positive when the line node i is over the seabed S, whereas $\boldsymbol{d_{P,i}}$ will be treated as positive if it points towards the sea surface. The two terms are obtained for each mooring line node by a continuous projection method described in the following sections.

2.2.2. Adaptation of the projection method to the type of seafloor surface

The proposed projection method is suitable to be applied at any type of seafloor. However, if the surface is flat (inclined or horizontal), which are common models to represent the seabed, the general method can be replaced by a point-to-plane projection expression, reducing the computational cost required in the flat cases.

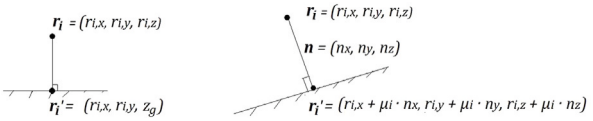

Fig. 3. Mooring line node $\boldsymbol{r}_i$ and its projection $\boldsymbol{r}'_i$ in two different seabeds. On the left, an horizontal seabed is shown, at height z_g. On the right, the inclined seabed.

2.2.2.1. Horizontal or inclined flat seabed. The horizontal flat seabed structure case is the simplest one: the direction of projection will always be the z-axis for every line node, so $\boldsymbol{d}_{\boldsymbol{P},i} = \boldsymbol{e_3}\ \forall i$. The distance between the mooring line nodes and the ground can be obtained by $d_{G,i} = r_{i,z} - z_g\ \forall i$, being z_g the seafloor height in the system of reference and $r_{i,z}$ the z-coordinate of the position of the node i, $\boldsymbol{r}_i$.

When the seabed surface is an inclined plane, the process starts by calculating the unitary normal vector of the plane $\boldsymbol{n}$ with three not aligned points. The plane satisfies the equation $\boldsymbol{P} \cdot \boldsymbol{n} = k$, being $\boldsymbol{P}$ a point contained in the plane. The normal vector of the inclined plane which models the seabed surface is the direction of projection for every mooring line node, $\boldsymbol{d}_{\boldsymbol{P},i} = \boldsymbol{n}\ \forall i$. To obtain the projected mooring line nodes coordinates, the following process was developed:

Let $\boldsymbol{r}'_i$ be the position of the projected line node i. $\boldsymbol{r}'_i$ is contained in the inclined plane and satisfies its equation:

$$\boldsymbol{r}'_i \cdot \boldsymbol{n} = k \tag{8}$$

$\boldsymbol{r}'_i$ is contained in the line with direction $\boldsymbol{n}$ that also contains $\boldsymbol{r}_i$, the line node position vector. Therefore, it satisfies the following parametric equation:

$$\boldsymbol{r}'_i = \boldsymbol{r}_i + \mu_i \boldsymbol{n} \tag{9}$$

Joining both Eqs. (8) and (9), for each mooring line node i, it is obtained that $\mu_i = k - \boldsymbol{r}_i \cdot \vec{n}$, allowing to calculate $\boldsymbol{r}'_i$ by replacing the term μ_i in Eq. (9). $d_{G,i}$ will be calculated by the expression $d_{G,i} = \alpha \|\boldsymbol{r}'_i - \boldsymbol{r}_i\|$ being $\alpha = sign(r_{D,z})$, with $\boldsymbol{r_D} = \boldsymbol{r}'_i - \boldsymbol{r}_i$ and $r_{D,z}$ its z-coordinate (see Fig. 3).

2.2.2.2. Complex bathymetries. When the seabed surface is neither horizontal or plane, several difficulties appear. The first concern is the interpretation of the seabed surface, which can be carried out by triangulating the seafloor surface. In order to avoid an unnecessary computational cost, the surface should be described in the least triangles needed. To be able to construct the triangulation, the seabed surface must be firstly described by several points. Then, a Delaunay triangulation (Lee and Schachter, 1980) using all the mentioned points as vertexes of different triangles is created.

A second problem to treat is the necessity of obtaining a projection direction which varies continuously. This is crucial to avoid computational problems in the calculation of the jacobian needed for the temporal simulation.

The proposed method uses an algorithm to project into a triangulated surface (in this case, the seabed surface). This projection tool was developed by Orazi and Reggiani (2020), and it is based on the vertex normals, the mean of the adjacent triangle normals in each vertex, instead of the normals of each triangle. This ensures a continuous variation of the projection direction. Before starting to project, it is computationally profitable to construct a change-of-frame matrix $\boldsymbol{M}$ for each of the triangles that form the triangulation of the seabed surface. $\boldsymbol{M}$ is composed by a series of translations and rotations that end up laying the chosen triangle into the XY plane, simplifying the projection process. It should be noticed that $\boldsymbol{M}^{-1}$ must be also calculated in order to return to the usual system of reference.

The projection process then starts by selecting a mooring line node and one of the triangles which describe the seafloor surface. Both the line node and the chosen triangle are moved to the layed triangle frame with its matrix $\boldsymbol{M}$. The next step is to check whether the mooring line node is inside the selected triangle or not. To do that, Optimized FCP algorithm is used (Orazi and Reggiani, 2020), which uses the barycentric coordinates (s, t) of the mooring line node inside the triangle. This process should be repeated for each triangle until the selected node is inside one of them. When this happens, the direction $\boldsymbol{d}$ is calculated:

$$\boldsymbol{d} = \boldsymbol{n_0} + (\boldsymbol{n_1} - \boldsymbol{n_0})s + (\boldsymbol{n_2} - \boldsymbol{n_0})t \tag{10}$$

The equation was taken from Orazi and Reggiani (2020). $\boldsymbol{n_0}, \boldsymbol{n_1}$ and $\boldsymbol{n_2}$ are the normal vertexes of the selected triangle in the layed triangle change of frame. Therefore, being i the mooring line node, its direction of projection is calculated by $\boldsymbol{d}_{\boldsymbol{P},i} = \boldsymbol{d} \cdot \boldsymbol{M}^{-1}$. The distance between the mooring line node and the seafloor surface can be obtained as the z coordinate of the line node when it is moved to the XY frame. For each line node i, this value corresponds to $d_{G,i}$.

The developed algorithm selects a mooring line node and iterates over the triangles which describe the seafloor surface until it is projected inside one. However, this can result in an unnecessary computational cost if the desired triangle is the last one checked.

The computational cost can be reduced by adding a list of triangles for each line node ordered by the distance between the triangle centroid and the node. Then, if the method iterates following the list, the searched triangle will be found sooner. The triangle list order is computed automatically based on the static solution, and it has to been updated for each node and for each time iteration. As future work, this list could be computed only once at the start of the simulation when the floor line nodes displacements are not large. This improvement is highly profitable when the number of triangles is large; in other case, ordering the list can have a higher computational cost than going through in the entire list of triangles.

2.2.3. Application to the calculation of forces

Once $\boldsymbol{d}_{\boldsymbol{P},i}$ and $d_{G,i}$ have been calculated for every mooring line node, it is possible to obtain the ground normal and friction forces for any type of seabed surface.

- Ground normal force

The implementation chosen for the ground normal force was a combination of the models developed by Palm et al. (2013) and Trubat et al. (2020). Both of them are based on a spring damper system and consider a flat seafloor. However, some changes were introduced to adapt it to an irregular seafloor surface. The direction of the force was set to $\boldsymbol{d}_{\boldsymbol{P},i}$ defined in Eq. (6) instead of following the z-axis, while the distance between the mooring line node and the seafloor was replaced by $d_{G,i}$. The expression obtained for a certain mooring line node i is the following:

$$\boldsymbol{f_n} = -d G_K \boldsymbol{d_G} - 2G_c \sqrt{G_K d \gamma_0} min(0, v_n) \boldsymbol{d}_{\boldsymbol{P},i} + \|p_n\| \boldsymbol{d}_{\boldsymbol{P},i} \tag{11}$$

being d the line diameter, γ_0 the mooring mass per length, G_K the ground normal stiffness per unit area and G_C the fraction of critical damping (will be taken as 1 from now on). $\boldsymbol{d_G}$ is the ground penetration for the selected line node, $\boldsymbol{d_G} = d_{G,i} \boldsymbol{d}_{\boldsymbol{P},i}$, while v_n is the velocity normal to the seafloor $v_n = \boldsymbol{v} \cdot \boldsymbol{d}_{\boldsymbol{P},i}$. Finally, the component associated to the equilibrium ground normal force opposing the line weight, $\|p_n\|$, is given by the expression $\|p_n\| = |\boldsymbol{p} \cdot \boldsymbol{d}_{\boldsymbol{P},i}|$. $\boldsymbol{p}$ is the line's submerged weight, defined by $\boldsymbol{p} = \left(1 - \frac{\gamma_W}{\gamma_0}\right) \gamma_0 \boldsymbol{g}$, being γ_W the mooring mass per length under water and $\boldsymbol{g} = -g\boldsymbol{e_3}$, with $g = 9.8\ \mathrm{m/s^2}$ the scalar value of Earth's gravity.

- Friction force

The friction force direction is contained in the seabed surface and opposes the movement. The description of the force is based on Devries and Hall (2018) saturated damping model, which considers the seafloor as flat. In order to model the interaction with an irregular

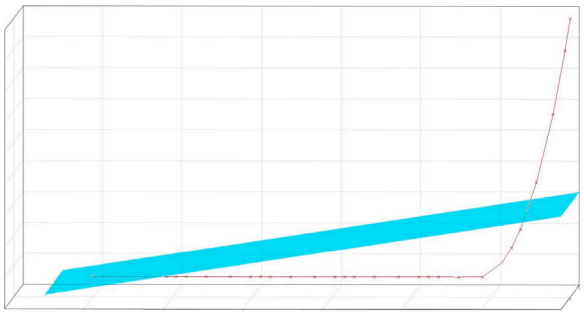

Fig. 4. Using the static approach for a catenary line on a sloped seabed can result in a buried mooring line, which is not realistic.

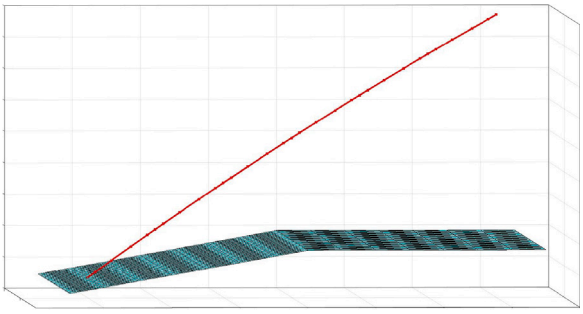

Fig. 5. The initial mooring line configuration of Newton–Armijo method $\boldsymbol{r}^{(0)}$ should be carefully selected. Otherwise, it could reach the static equilibrium at the inverse catenary.

seabed surface, the velocity in the plane XY is replaced by the velocity perpendicular to $\boldsymbol{d}_{P,i}$.

$$\boldsymbol{f}_f = \begin{cases} -C_k \|\boldsymbol{f}_n\| \frac{\boldsymbol{v}_\pi}{v_c}, & \text{if } \|\boldsymbol{v}_\pi\| < v_c. \\ -C_k \|\boldsymbol{f}_n\| \frac{\boldsymbol{v}_\pi}{\|\boldsymbol{v}_\pi\|}, & \text{otherwise.} \end{cases} \tag{12}$$

being C_k the kinetic friction coefficient, v_c a velocity threshold (a scalar) and $\boldsymbol{f}_n$ the previous calculated normal force. $\boldsymbol{v}_\pi$ is the velocity contained in the seafloor surface plane, and can be obtained by $\boldsymbol{v}_\pi = \boldsymbol{v} - v_n \boldsymbol{d}_{P,i}$, where $\boldsymbol{v}$ is the total velocity of the line node and v_n is defined as in the ground normal formulation.

2.3. Initial condition problem

The mooring simulation is based on finite element method which uses stiffness and mass matrices, and therefore depends on an initial condition that can be found by a static approach.

Before implementing an irregular seabed bathymetry, the static approach was defined as the catenary between the fairlead and the anchor. However, this situation does not represent a reliable initial condition when the seafloor is not flat because there could be buried parts, as it is shown in Fig. 4. This will increase tensions and move away from a realistic behavior. Therefore, the catenary static approach was changed to the static equilibrium of the mooring line.

The static equilibrium is found using Newton–Armijo (Kelley, 2003) iterative method, which is capable of solving non-linear systems in the form $\boldsymbol{F}(\boldsymbol{r}) = \boldsymbol{0}$, where $\boldsymbol{r}$ contains the mooring line nodes positions and $\boldsymbol{F}(\boldsymbol{r})$ is the vector containing the forces in those positions. The algorithm reaches the equilibrium when the relative error between the iterations is lower than 10^{-3}.

Newton–Armijo method needs to start the iteration with a mooring line positioning ($\boldsymbol{r}^{(0)}$) in which a good convergence is ensured. This is achieved by choosing $\boldsymbol{r}^{(0)}$ as a catenary between the anchor and the fairlead. Using other mooring line positioning as Newton–Armijo method initial point can lead to reach the static equilibrium at the inverse catenary as it can be seen in Fig. 5, which is not realistic. This is what happened when line between the fairlead and the anchor was taken as the point to start the iterations.

2.4. Discretization problem

The described method projects the FEM nodes in which the mooring line is divided into the seabed surface. If the mooring line is not well discretizied in accordance to the irregularities of the seafloor, the seabed surface cannot be well interpreted as shown in Fig. 6:

The number of mooring line nodes needed depends on the irregularities of the seabed: if it is too tight or complex, the number of nodes in which the mooring line is divided must be larger. However, elevating the number of nodes will enlarge exponentially the duration of the simulation. In order to select a good number of nodes and avoiding the mentioned problems, a sensitivity analysis must be performed, studying the point of convergence of the fairlead tension for different discretizations. For the case described above, the following results were obtained:

It can be seen that using a discretization of 75 nodes, convergence is achieved in the presented case. However, most of the seafloors are simpler, and it is not necessary to use such a large amount of nodes. The dynamic differences between the number of nodes would have been stronger than the ones in Table 1 if the size of the step had been bigger. Nevertheless, this section is focused in the importance of the mesh definition rather than in the dynamics of the mooring line.

As expected, the computational time increases fast with the number of nodes. This happens because the size of the PDE describing the mooring line dynamics increases, and solving it requires more time. In addition, using a large quantity of triangles to describe the seafloor surface increases the computational time. To perform a more efficient simulation, local mesh refinement can also be applied in areas with narrow irregularities on the seabed.

3. Analytical verification

The results obtained by the developed method can be compared with the analytical expression of a catenary in a slope provided by Batista and Perkovic (2019). In their work, they modeled a static mooring system (fairlead position $\boldsymbol{r}_F$ is fixed to a point) anchored to an inclined seabed. As the seafloor is inclined, the projection method used in the simulation will be the point-to-plane projection described in Section 2.2.2.1. This comparison gives a measurement of the accuracy of the numerical simulation, in particular, to its capacity to model a mooring laying on an inclined plane.

In their article, Batista and Perkovic (2019) introduce a two dimensional mooring line which lays into an inclined plane and is subjected to an external known force H. This external force is applied to the fairlead and it elevates the mooring line, which starts to behave as a catenary from a touchdown point $\boldsymbol{P_1}$. The mooring is anchored to the inclined plane and its other extreme, the fairlead, does not move. Regarding the description of the forces involved, Batista and Perkovic (2019) treat the mooring line as inextensible, the ground as impenetrable and ignore friction effects. The described situation is represented in Fig. 7.

The frame of reference is defined the same way as in the previous Section 2.1, but in this case it is restricted to the plane y = 0 in order to achieve a bidimensional numerical simulation.

Most of the parameters used to characterize the mooring line have been chosen in accordance to the parameters that will be later used in the experimental validation, as it can be seen Tables 2 and 5. Young's Modulus multiplied by the catenary area (EA), which appears in tension description shown in Eq. (2), was highly increased in order to model an inextensible mooring line. On the other hand, the floor can be modeled as impenetrable by enlarging the parameter G_K in the ground normal force described in Eq. (11) up to $3 \cdot 10^{14}$ N/m^3.

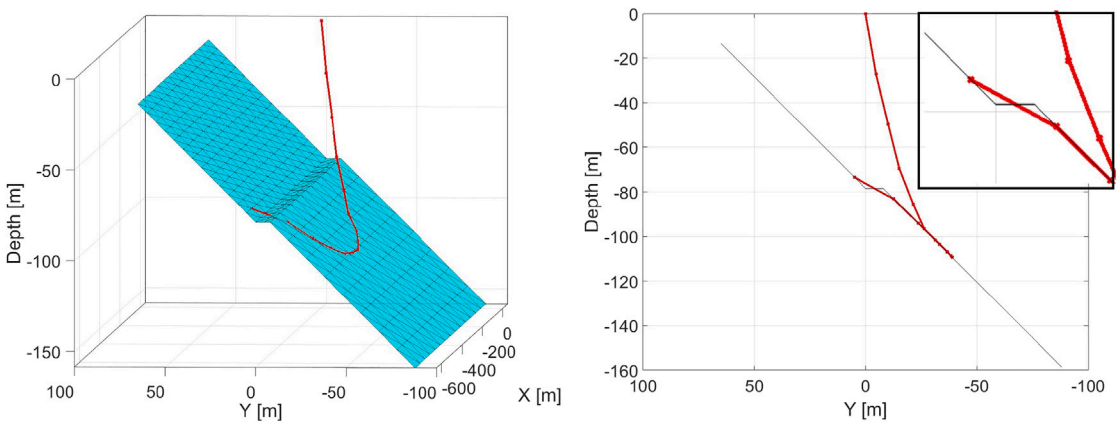

Fig. 6. In the presented seabed surface (blue), there is a small step in the middle of an inclined plane, but there are no mooring line nodes laying on it, causing a bad interpretation of the seabed structure. The mooring line presented in this figure is divided into 15 nodes.

Table 1
An example of a sensitivity analysis for the situation described in Fig. 6 in which the fairlead tension is compared to the discretization. The computational time ratio is also shown, which is the quotient between the computational times required for the studied case and for the one with 15 nodes.

Nodes	15	25	35	45	55	65	75	85
Fairlead Tension [N]	$3.13 \cdot 10^6$	$3.24 \cdot 10^6$	$3.18 \cdot 10^6$	$3.10 \cdot 10^6$	$3.19 \cdot 10^6$	$3.06 \cdot 10^6$	$3.10 \cdot 10^6$	$3.10 \cdot 10^6$
Computational time ratio	1	1.79	4.01	5.59	10.30	13.57	18.13	24.66

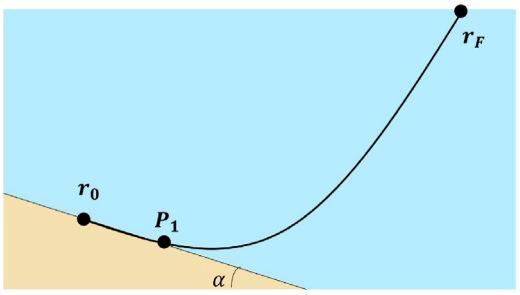

Fig. 7. Scheme of the situation proposed by Batista and Perkovic (2019). α is the plane inclination. The mooring is anchored to the inclined plane at $\boldsymbol{r_0}$ and the fairlead, $\boldsymbol{r_F}$, is static. $\boldsymbol{P_1}$ is the point where the mooring line starts to elevate from the ground.

Table 2
Characterization of the mooring line.

Abbreviation	Parameter	Value
L	Length [m]	635
γ_0	Weight per unit of length [kg/m]	835.4
d	Line diameter [m]	0.3539
EA	Young's Modulus multiplied by area [N]	$5 \cdot 10^{11}$
β	Coefficient of the internal damping coefficient as function of EA	0.005
C_{Dn}	Normal Drag Coefficient	2.5
C_{Dt}	Tangential Drag Coefficient	0.5
C_{MN}	Added mass Coefficient	3.8
ρ_W	Water density [kg/m^3]	1025
G_K	Ground normal stiffness per unit area [N/m^3]	$3 \cdot 10^{14}$

3.1. Results comparison

Firstly, the position of the analytical solution provided by Batista and Perkovic (2019) and the positions of the mooring line nodes returned by the numerical simulation were compared. In addition, a second analysis was consisted of comparing the fairlead tension obtained numerically by the simulation and the one given analytically was performed.

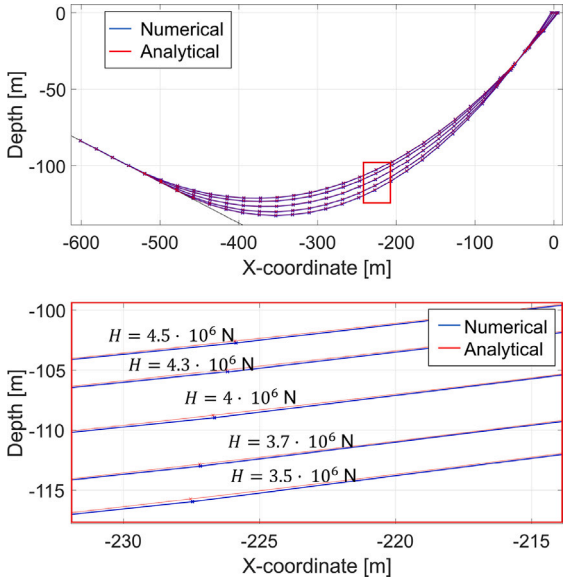

Fig. 8. Comparative between the analytical expression obtained from Batista and Perkovic (2019), in red, and the mooring line nodes positions obtained from the numerical simulation, in blue. The inclination of the seabed surface to which the mooring line is anchored is $\alpha = 15°$. The figure below is a magnification.

3.1.1. Position comparison

The comparison between the mooring line nodes positions and the coordinates of the analytical solution was performed for different values of external horizontal force H. Fig. 8 shows the obtained results:

The differences between the analytic and numerical solutions were quantified in Table 3. As the number of nodes in which the mooring line has been discretized is 32, only certain of them are shown in Table 3. In particular, the selected nodes correspond to the rounded value of the nth percentile of the list of them, with $n \in \{10, 20, \ldots, 90\}$. Node

Table 3
Absolute difference (in meters) between the numerical and analytic results for certain mooring line nodes. The difference in the index (i, j) is associated with the node j and has been calculated as $\Delta = \sqrt{\Delta_x(j)^2 + \Delta_z(j)^2}$, where $\Delta_x(j)$ is the absolute difference between the numerical and the analytical values of the x-positions of the jth node, and $\Delta_z(j)$ is the same count with the z-positions.

H [N]	Node								
	2	6	9	12	16	19	22	25	29
$4.5 \cdot 10^6$	0.031	0.085	0.042	0.159	0.169	0.182	0.129	0.23	0.249
$4.3 \cdot 10^6$	0.014	0.051	0.039	0.162	0.185	0.187	0.148	0.237	0.255
$4 \cdot 10^6$	0.023	0.012	0.064	0.167	0.211	0.142	0.178	0.208	0.255
$3.7 \cdot 10^6$	0.014	0.123	0.029	0.178	0.177	0.2	0.125	0.255	0.275
$3.5 \cdot 10^6$	0.017	0.078	0.037	0.161	0.231	0.181	0.204	0.244	0.277

Table 4
Relative error ($\delta T = |T_S - T_A|/T_A$) between the analytical fairlead tension (T_A) and the one obtained from the numerical simulation (T_N) for different horizontal external forces H.

H [kN]	T_N [kN]	T_A [kN]	$\lvert T_N - T_A \rvert$ [kN]	δT
3500	5369	5373	4	0.0007
3700	5184	5188	4	0.0008
4000	4915	4912	3	0.0006
4300	4633	4637	4	0.0009
4500	4453	4454	1	0.0002

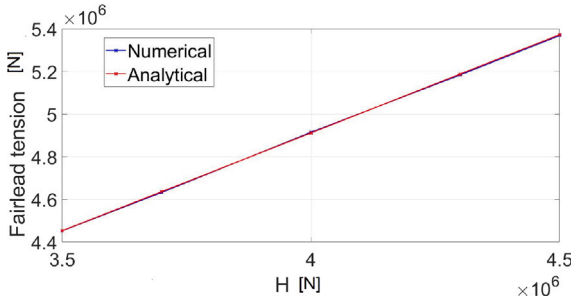

Fig. 9. Comparative of the fairlead tension obtained from the analytical expression and the one obtained from the numerical simulation for different values of H.

number 0 corresponds to the anchor while node number 31 represents the fairlead.

3.1.2. Fairlead tension comparison

For the same values of the external horizontal force H as the ones used before, it was possible to compare the fairlead tension calculated with the analytical expression provided by Batista and Perkovic (2019) with the values obtained numerically.

3.2. Discussion of the results

The results show great accordance between the analytical solution and the one obtained by the numerical method, proving the good behavior of the developed point-to-plane projection method.

Table 3 shows that the absolute differences between both analytical and numerical solutions differ quantities lower than 0.3 m. Regarding the total length of the mooring line, 635m (see Table 2), it can be traduced to errors lower than 0.05% of the mooring length. This error is of the same order of magnitude that allowed by Newton–Armijo's method discussed in Section 2.3. In Table 3 it can be seen that the mooring line nodes located near the anchor show even smaller differences between both solutions.

This high accordance is also shown in Fig. 8, where the graphs of both solutions almost overlap. With certain effort, it can be distinguished that the numerical simulation is slightly below the analytical expression. This error is due to the impossibility of achieving an absolutely inextensible mooring line, which only could be reached if

Table 5
Characterization of the mooring line. Most of the coefficients determination were based on the studies of Palm et al. (2017): the water density, the normal and tangential drag coefficients, the added mass coefficient or the ones related with friction force (velocity threshold and kinetic friction coefficient). The ground normal stiffness was taken from Barrera et al. (2020). The mooring line length, diameter, weight, Young's Modulus multiplied by area and internal damping coefficient have been chosen in accordance to Mahfouz et al. (2020).

Abbreviation	Parameter	Value
L	Length [m]	635
γ_0	Weight per unit of length [kg /m]	835.4
d	Line diameter [m]	0.3539
EA	Young's Modulus multiplied by area [N]	$3.15 \cdot 10^9$
β	Coefficient of the internal damping coefficient as function of EA	0.001
C_{Dn}	Normal Drag Coefficient	2.5
C_{Dt}	Tangential Drag Coefficient	0.5
C_{MN}	Added mass Coefficient	3.8
ρ_W	Water density [kg/m^3]	1025
G_K	Ground normal stiffness per unit area [N/m^3]	$3 \cdot 10^5$
v_c	Velocity threshold [m/s]	0.01
C_K	Kinetic friction coefficient	0.3

Young's Modulus (EA) was set to infinity. However, it must be a finite parameter, introducing certain error. Although the value could not be infinite, it was set to $5.055 \cdot 10^{11}$ kg/s^2 m (Table 2) which is more than a hundred times higher than the experimental used value $3.15 \cdot 10^9$ kg/s^2 m (Table 5). This selected value is high enough to simulate the desired inextensible behavior, as the results show.

The error produced by not achieving a complete inextensible mooring line would have been even lower if the simulated mooring was shorter and softer. However, one of the objectives was to validate the experimental set up, so the characterization of the parameters of the mooring line in this section should be as similar as possible to the one described in the experimental validation section, as it was previously discussed.

Finally, both Table 4 and Fig. 9 show great accordance, giving relative errors in fairlead tensions lower than 10^{-3}. It can be seen that the relative error is not homogeneous, as it is higher in some cases and lower in other ones. This could be due to the convergence criteria used for the Newton–Armijo method. However, in all of the cases, it can be concluded that the results are really accurate.

4. Experimental validation

4.1. Model test set up

In order to validate the proposed model, a single mooring line was subjected to forced oscillation scale tests, which have been conducted in the COCOTSU wave and current flume facility managed by the Environmental Hydraulics Institute. This device is 56m long, 2m wide and has a variable height between 1.8 m and 2.5 m. It is equipped with a wave generation system based on a 2m piston-type paddle, as well as with a wave dissipation system. However, the performed tests have been carried out without waves. Fig. 10 shows some flume views:

The mooring lines were simulated by means of chains, and located inside the flume. They were attached to the seabed by a steel plate that worked as an anchor, and moored to a linear actuator. Froude scaling laws were applied to reproduce the hydrodynamic behavior at model scale.

The mooring line used during the test program can be characterized by the following characterization:

As the intention of the tests is to verify the accuracy of the simulation of a mooring line in a variable seabed surface, the mooring tests were repeated into three different surfaces described in Fig. 11, which

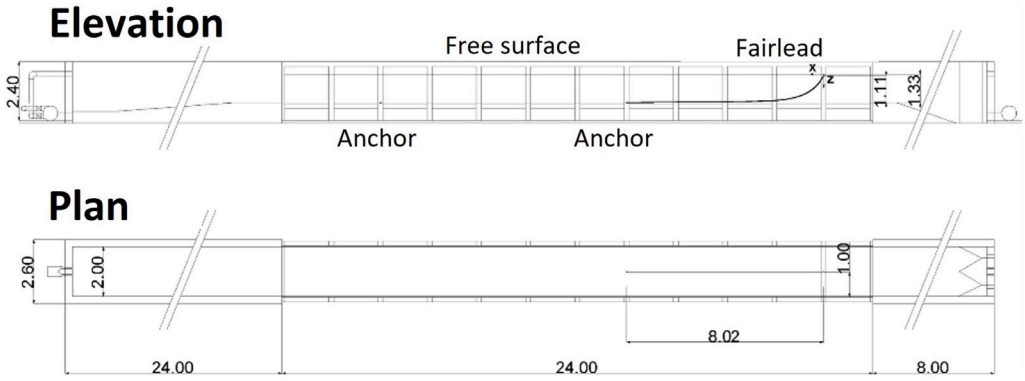

Fig. 10. Elevation and plan views of test layouts. The used scale is 1 : 75.

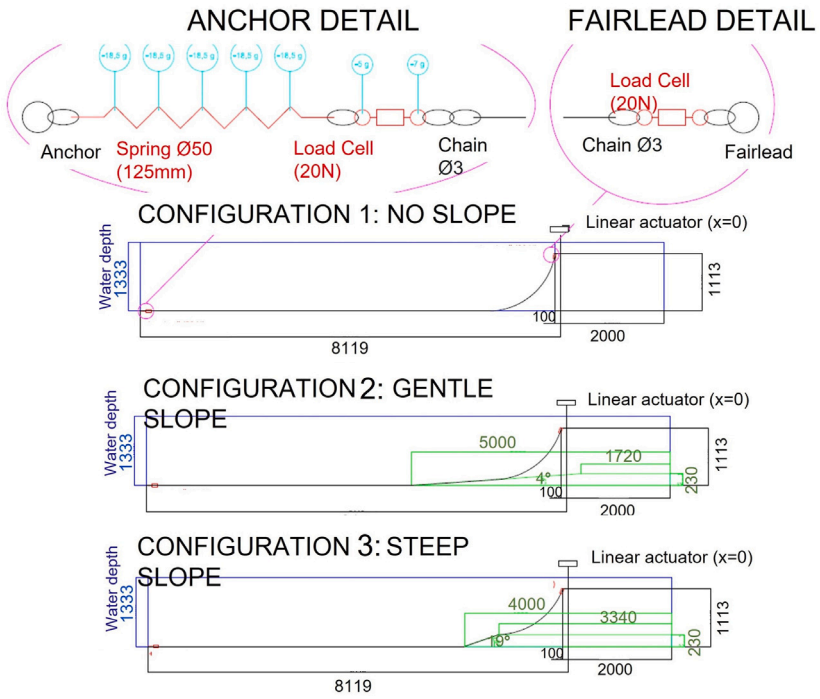

Fig. 11. Three different sloped seabed configurations, from top to bottom: no-slope, gentle-slope (4° of inclination) and steep-slope (19° of inclination). The used scale is 1 : 75.

are no-slope, gentle-slope (4°) and steep-slope(19°) cases. The location of the step, as well as its length, vary for the three tested seabed types. In addition, the main difference between the sloped cases is that the gentle-slope case is dominated by the interaction with the line into its bottom concave corner whereas the steep-slope case is dominated by the interaction with its top convex corner. This variations allow to properly study the dynamics of contact.

For the sloped steps, Fig. 11 shows that the seabed structure is described as a mixture of flat and inclined floor pieces, and it cannot be described as only one of them. This way, the projection method used was the general one, able to describe any type of seabed surface. Comparing the precision of the results between the sloped and no-sloped cases will determine whether the introduction of this method increases the discrepancies between the numerical and the experimental results or not.

In Fig. 11, it can be seen the two axial load cells used in both the anchoring and fairlead points. The TECSIS F2808 forced transducers used at 100 Hz have an accuracy of 0.1% of their force, 20N. They are used to identify the dynamic performance and snap tensions of the mooring line. In addition, to make the mass of the anchoring point per unit length the same as that of the chain underwater, floats are added at its axial load cell.

The linear actuator Bosch:ECM80 was used to impose different harmonic movements to the fairlead. It reaches an acceleration of 9.5 m/s^2 and a maximum force of 600N, and it is supported by an aluminium structure built inside the flume.

For each of the three cases, two different tests comparing the numerical (num.) and experimental (exp.) results were performed. The first one corresponds to a fairlead imposed movement of low frequency, with 17 s of period, a mean drift of 15 m and an amplitude of 2.5 m. This condition allows to model a quasistatic performance case because gradients of fairlead tensions follow the gradient of surge displacements, as it can be seen in the Figs. 12, 14 and 16. Hence, the dynamic effects are low, allowing these tests to validate the model without snapping loads.

In the second case, the fairlead oscillations frequency increases up to a period of 6 s, while their amplitude reaches 5 m. Also, the fairlead movement has no offset. This time, as the Figs. 13, 15 and 17 show, the fairlead tension peaks are not located at the maximum surge position but at its maximum velocity, which is reached when the surge gradient changes it sign. The described situation aims to validate the model with snapping loads and to evaluate the dynamic performance of the mooring line. Therefore, it is expected to have a higher sensibility to

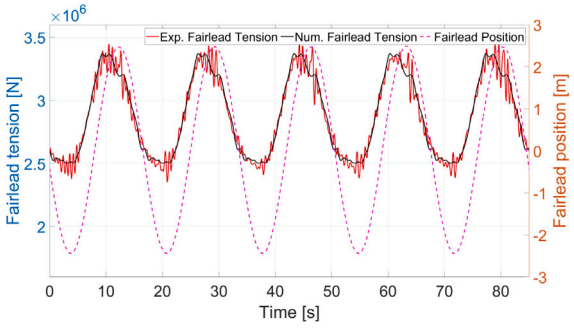

Fig. 12. Fairlead tension time series with amplitude of 2.5 m, a mean drift of 15 m and period of 17 s for the no-slope configuration.

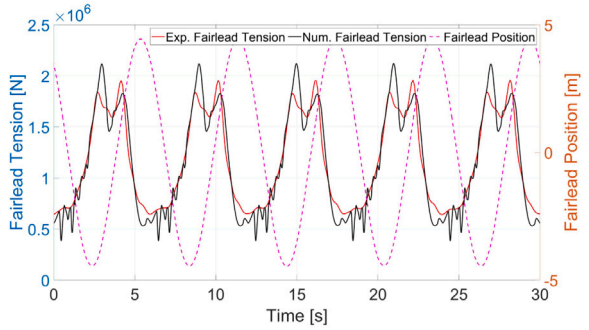

Fig. 13. Fairlead tension time series with amplitude of 5 m, no offset and period of 6 s for the no-slope configuration.

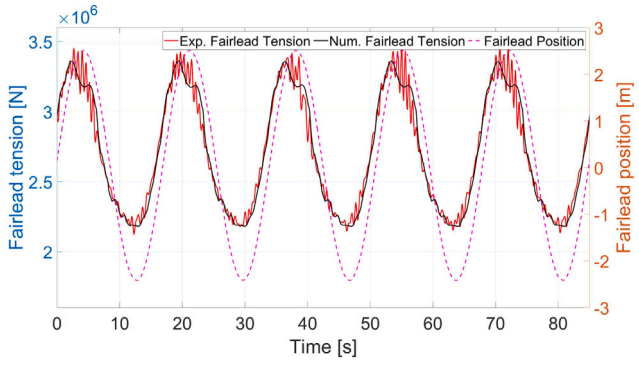

Fig. 14. Fairlead tension time series with amplitude of 2.5 m, a mean drift of 15 m and period of 17 s for the gentle-slope configuration.

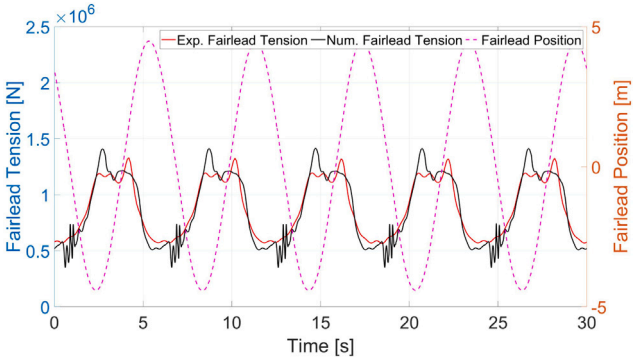

Fig. 15. Fairlead tension time series with amplitude of 5 m, no offset and period of 6 s for the gentle-slope configuration.

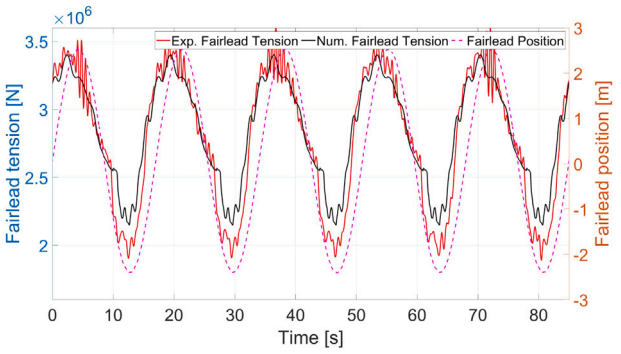

Fig. 16. Fairlead tension time series with amplitude of 2.5 m, a mean drift of 15 m and period of 17 s for the steep-slope configuration.

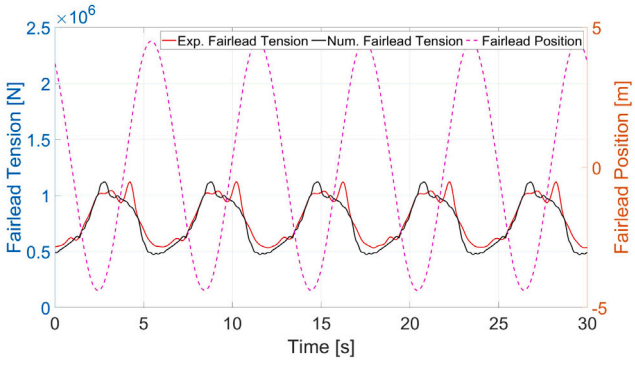

Fig. 17. Fairlead tension time series with amplitude of 5 m, no offset and period of 6 s for the steep-slope configuration.

the seabed contact than the previous configuration. With the results obtained for the six described cases, the following fairlead tension temporal series were obtained:

The agreement of the numerical and experimental results overall is limited by the scaling effects, specially by the introduction of a spring at the anchor in the experiment in order to reproduce the line stiffness properly, as it can be seen in Fig. 11. The introduction of a sloped seabed does not affect the agreement.

In the quasi-static performance, the lowest tension peak value differs in the three different configurations of the seabed. For the flat seabed (Fig. 12), its value is around $2.5 \cdot 10^6$ N. In the case of the gentle-slope configuration (Fig. 14), its value decreases up to $2.2 \cdot 10^6$ N and finally, in the steep-slope seabed (Fig. 16), it decreases again achieving a value of $2 \cdot 10^6$ N. However, the different values of the experimental lowest tension peak are well-captured by the numerical simulation, although the numerical results of the steep-slope case show a slightly worse result. This happens because the mooring line discretization in this case does not allow to capture the contact between the line and the seafloor with all the possible precision. In the case with a horizontal seafloor, it was found a higher tension than in the other cases. This is because the portion of the mooring line that touches the seafloor is lower when the seafloor is horizontal than when an inclination is introduced.

In the dynamic performance, the fairlead tensions are higher in the flat seabed configuration (Fig. 13), decrease when the gentle-slope configuration is considered (Fig. 15) and decrease even more when the studied case is the steep-slope (Fig. 17). This behavior is expected due to the increment in the fraction of the mooring line touching the seafloor, as it was previously explained. In addition, the numerical results do perfectly couple with these decreases in tension for all cases.

Finally, as it was anticipated, the tension differences between the different seabed configurations are higher in the dynamic performance

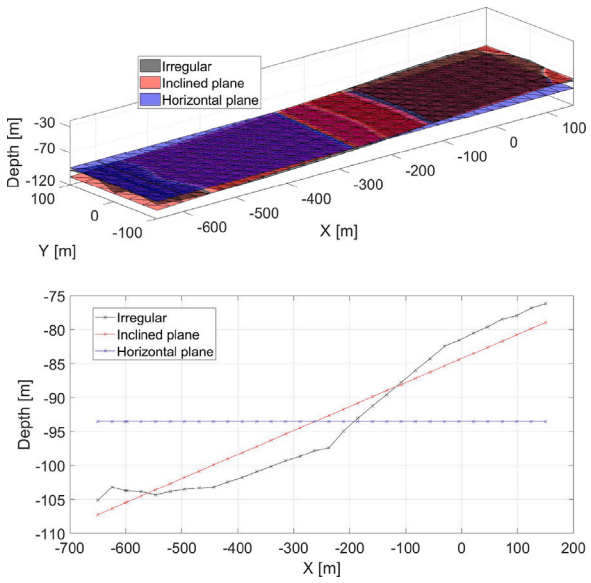

Fig. 18. Irregular surface generated with diamond-square algorithm (blue), its interpolation by an inclined plane (green) and its approximation by an horizontal plane of depth $\bar{z} = -93.5$ m (red). The figure below shows a cut from the figure above at the plane y = 0.

than in the quasi-static performance. Nevertheless, the total tensions of the quasistatic performance are higher because in them, the fairlead movement had an offset which made the mooring line more tense.

In conclusion, the agreement between the numerical and the experimental results for both the sloped-cases is similar to the one obtained with a flat seabed, allowing to successfully validate the implementation of the complex bathymetry model.

5. Effect of the variable bathymetry

In this section, an irregular and inclined seabed surface is studied. It was created using the Fractal landscape generator with diamond-square algorithm (Kaya, 2022), which is a common tool for developing realistic landscapes for videogames graphics. The algorithm depends on certain parameters: the resolution, the amplitude of the irregularities and the smoothness. This last parameter is a value between 0 and 1, when the closer it is to 0, the smoother is the surface. The selected value was 0.3.

A mooring located in this surface can be modeled in various ways. The first one consists of using the projection algorithm developed for irregular bathymetries, which needs the seabed surface coordinates as a parameter. These coordinates are obtained by the previous cited diamond-squared algorithm (Kaya, 2022). Another possible interpretation of the situation is to treat the irregular surface as an inclined plane, which can be achieved by interpolating the seabed surface by a plane. This approximation allows to use the described point-to-plane projection method for inclined seabed surfaces. Finally, the mean of the depth of all the points forming the seabed surface can be calculated ($\bar{z}$) and the irregular surface can be approximated by an horizontal plane located at $\bar{z}$. In this case, it is used the projection method for horizontal seafloors.

Studying the solutions obtained by these three methods allow to calculate the numerical differences in their positions as well as in their fairlead tensions. The magnitude of these differences will determine the importance of considering an irregular bathymetry rather than approximating it by an horizontal seabed surface, which has been the method used so far.

As it can be seen in Fig. 18, there are irregularities along both X and Y axis. In order to evaluate their impact, the fairlead was imposed to describe a circular movement in the plane XY of amplitude 2.5 m, a period of 12 s and its origin at $x = 10$ m, $y = 0$ m. The mooring line characterization has been chosen as the same described in Table 5. Once the numerical simulations were performed, each of them with their corresponding method of projection, the positions of the mooring line nodes obtained at a certain fixed time were compared:

In the case in which the true seabed is considered, in Fig. 19 it can be seen that the fairlead movement can rise a big part of the mooring line from the seabed. For the inclined and the horizontal seabeds, the rise is more gradual. In addition, the predicted touchdown point will be different in each of the three cases. This has a big impact in line stiffness, as it was concluded by Jaiswal et al. (2016).

The fairlead tensions for each of the three methods have also been analyzed. In Fig. 20, fairlead temporal tension series for the three different approaches used in this problem are represented. Both total and dynamic tensions have been calculated. The total tensions are the natural measurements while the dynamic tensions have been obtained by subtracting the correspondent pretension, which has been calculated as the average of the total tensions in each of the cases.

Dynamic fairlead tension series in Fig. 20 allow to compare the three methods without considering initial pretensions. In them, the irregular treatment case shows a higher peak tension, reaching a value of $5 \cdot 10^5$ N, than the other two approximations, whose peak is lower than $4 \cdot 10^5$ N. This is coherent with the previous discussion done for the position results exposed in Fig. 19, which concluded that the touchdown point and the fast change of the part of the mooring line that is rised from the seabed produced a high impact on line tensions.

Fig. 20 also shows total fairlead tension series, which provide an interesting conclusion: the horizontal approximation has a higher total tension than the inclined plane approach. The horizontal approximation total peak reaches $2.4 \cdot 10^6$ N while the inclined plane approximation keeps in $2.2 \cdot 10^6$ N. This difference appears not only in the highest peak, but also in the whole temporal series. This is because the horizontal case depth, $\bar{z}$, has been calculated with the mean of the z-positions obtained by applying the diamond-square algorithm (in other words, the ones used to describe the irregular seabed surface) instead of the points where the mooring is really touching the seafloor. Then, the horizontal seafloor depth is higher than it should be, making that a higher fraction of the mooring line is raised, increasing the total tension. In addition, Fig. 19 shows that the touchdown point of the inclined plane surface is higher than the one in horizontal seabed, which explains that the total tension of the horizontal case is higher than the one in the inclined plane. In addition, the total fairlead tension obtained for the irregular case is the highest one, in coherence with the previous analysis. Its peak values $2.8 \cdot 10^6$ N.

Another relevant aspect that should be discussed is the increase in computational time caused by the use of the projection algorithm developed for general seafloor surfaces. For this task, the horizontal seafloor described in Fig. 18, located at a depth of $z = -93.5$m, was used. The mooring line characterization was the same as in the previous part of this section.

The mooring line simulation was performed using two different approaches. The first one consisted of using the point-to-plane projection method for horizontal seabeds. The second approach starts by triangulating the seafloor surface and using the general projection method. Therefore, all the difference in simulation time will be due to the projection algorithm used and not to other factors, such as the change in tensions that appears when different seafloor surfaces are introduced. The results obtained can be seen in Table 6.

The results show that the use of the developed projection method for irregular bathymetries increases the computational time around a 20%. This percentage is not very high, especially knowing that the accuracy of the simulation is greatly improved, as it has been previously discussed.

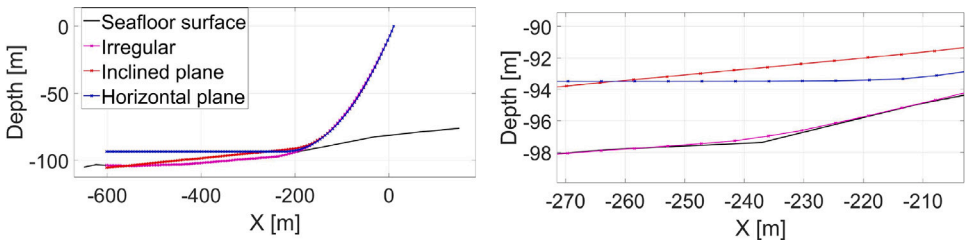

Fig. 19. Comparison of the obtained mooring line nodes positions for the three different cases at t= 6 s. Both figures show the cut at y= 0 from the surface presented in Fig. 18. The right figure is a magnification of the left one.

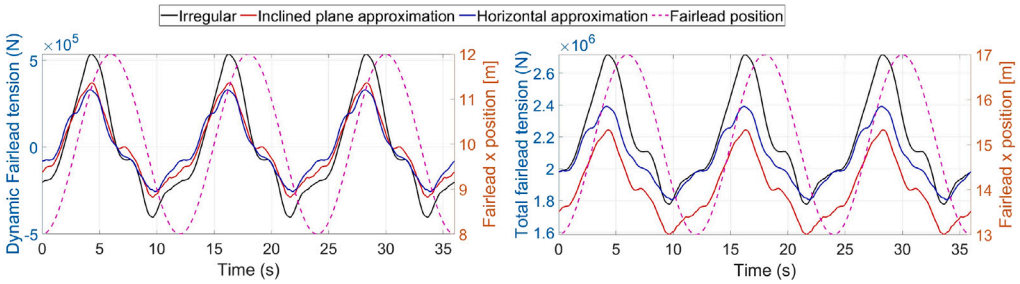

Fig. 20. Comparison of the fairlead tension series for the three described cases. In the left figure, the pretensions have been subtracted in order to calculate dynamic tensions. In the right figure, the total fairlead tension is being represented.

Table 6
Computational time required in a simulation of 120 s for two different projection algorithms. The mooring line and the seafloor were the same for both cases.

Projection algorithm	Computational time (s)
Specific for horizontal seabed	11236
General	13488

6. Conclusions

The presented work provides a method to simulate mooring lines in complex bathymetries.

(1) The method lays in a continuous projection that allows to calculate the parameters which describe the ground normal and the friction forces in a complex seafloor structure. The models used to implement these two forces are based on previous studies.

(2) The projection algorithm is able to distinguish whether the seafloor surface is flat (horizontal or inclined), where the projection process will be described as a point-to-plane projection, or if it describes a complex bathymetry, where a triangulation models the seafloor surface and the vertex normals are used to provide continuity to the projection method. An extra developed implementation allows to search the closest-barycenter triangle for a certain mooring line node before starting the projection process, which can reduce computational cost when the number of triangles used to describe the seabed surface is high.

(3) The initial condition problem was solved by searching the FEM static equilibrium with Newton–Armijo iterative method of solving non-linear systems. Newton–Armijo needs a first mooring line positioning to start its iterations, which was set as a catenary between the fairlead and the anchor. Other first configurations converged to the inverse catenary and were discarded. Using a catenary as the static approach is not correct in general when the seafloor is not flat. It could be observed that the line nodes should be increased when the seabed structure is complex.

(4) The method was verified with the analytical expression of a catenary in an inclined plane. In order to approach the simulation conditions as much as possible to the ones described in the article, the ground was made impenetrable by increasing the ground normal stiffness coefficient and the mooring was treated as inextensible by increasing Young's Modulus. The results showed extremely great accordance between the numerical obtained results and the analytic solution: the positioning comparison obtains relative errors lower than $5 \cdot 10^{-4}$ while the relative differences in the fairlead tension comparison are lower than 10^{-3}, having the same order of magnitude introduced by the Newton–Armijo convergence criteria.

(5) Several experimental scale tests were used to validate the accuracy of the proposed model. High frequency fairlead tests were used to validate the model with snapping loads while the low frequency movements aimed to validate the model without snapping loads. The comparison between the flat floor with the two different sloped tests allowed to validate different contact dynamics. The results confirmed that the introduction of a complex bathymetry did not affect the agreement of the numerical and experimental results. The proposed numerical model could predict the effect of the bathymetry on the line tension.

(6) A practical case of a mooring line over an irregular seabed surface was exposed. The results obtained numerically for three different proposed solutions were compared. At first place, the developed projection algorithm for complex bathymetries was directly applied. Then, the irregular surface was interpolated by an inclined plane and the projection method constructed to sloped seabed surfaces was used. By last, the mean of all the seabed surface points depth was used as the depth of an horizontal flat seafloor, being able to apply the projection method for horizontal seabeds. The differences between these three methods exalt the importance of considering a variable bathymetry. The general projection algorithm could predict fairlead tension: the dynamic fairlead tension peak in this case was $5 \cdot 10^5$ N while, in the other approximations it decreased until $4 \cdot 10^5$. The difference in the results comes from the prediction of the touchdown point, which varies the raised section of the mooring line and plays an important role in determining the line stiffness.

(7) In order to quantify the increase in computational time in the proposed method, a horizontal seafloor was triangulated. Then,

two different analysis were performed: the first one used the horizontal seafloor projection method, while the second was based in the general projection method. Is was found that the last one represents an increase in computational time of 20%.

In conclusion, the proposed model could be verified against an analytical solution as well as validated with different experimental scale tests. It can be concluded that the described implementation can be used to simulate mooring lines in complex bathymetries, highly improving the accuracy of the mooring line simulations which consider the seabed to be horizontal. This is specially valuable in certain locations in which the seafloor rapidly varies, such as in deep waters or in the Canary Islands. Working with irregular seafloor surfaces provides a big improvement in the calculation of friction and ground normal forces, improving the numerical results for both dynamic snap loads and line positioning. This allows to develop more secure devices and results in cost saving.

As further work, it is proposed to actualize the FEM used in the simulation, basing it in discontinuous Galerkin and using higher order finite elements.

It will also be interesting to contemplate other more complex friction model which take into account both static and dynamic friction. Furthermore, in an inclined plane, the friction is not isotropic, so a next possible step could be to implement a model able to reproduce an anisotropic friction. Also, the centroid-based order of the list of triangles used in the projection method developed for irregular surfaces could be optimized. Finally, coupling a line with a floating structure will allow to study the effect of variable bathymetries in complete mooring systems.

CRediT authorship contribution statement

Paula Desiré: Software, Formal analysis, Investigation, Validation, Writing – Original Draft, Visualization, Writing – Review & Editing. **Álvaro Rodríguez-Luis:** Methodology, Resources, Software, Formal analysis, Investigation, Writing – Review & Editing. **Raúl Guanche:** Conceptualization, Resources, Writing – Review & Editing, Supervision, Project administration, Funding acquisition.

Declaration of competing interest

The authors declare that they have no known competing financial interests or personal relationships that could have appeared to influence the work reported in this paper.

Data availability

Data will be made available on request.

Acknowledgments

This work is part of the COREWIND project which has received funding from the European Union's Horizon 2020 Research and Innovation programme under grant agreement No 815083, as well as part of OASYS Project Grant PDC2021-121786-I00 funded by MCIN/AEI/10.13039/501100011033 and by the European Union Next Generation EU/PRTR. Also, Raul Guanche would like to acknowledge the funding received from the Ramon y Cajal 2017 research program. GrantRYC-2017-23260 funded by MCIN/AEI/10.13039/501100011033 and by ESF Investing in your future". All authors approved the version of the manuscript to be published.

References

Aamo, O., Fossen, T., 2000. Finite element modelling of mooring lines. Math. Comput. Simulation 53, 415–422. http://dx.doi.org/10.1016/S0378-4754(00)00235-4.

Azcona, J., Munduat, X., González, L., Nygaard, T., 2017. Experimental validation of a dynamic mooring lines code with tension and motion measurements of a submerged chain. Ocean Eng. 129, 415–427. http://dx.doi.org/10.1016/j.oceaneng.2016.10.051.

Barrera, C., Guanche, R., Rodríguez, A., Armesto, A., Losada, I., 2020. On the importance of mooring system parametrisation for accurate floating structure designs. Mar. Struct. 72, 102765. http://dx.doi.org/10.1016/j.marstruc.2020.102765.

Batista, M., Perkovic, M., 2019. Computation of mooring chain with the touchdown on an inclined seabed. J. Mar. Eng. Technol. 21, 9–22. http://dx.doi.org/10.1080/20464177.2019.1572059.

Bonaventura, L., Gómez, M., 2021. The TR-BDF2 method for second order problems in structural mechanics. Comput. Math. Appl. 92, 13–26. http://dx.doi.org/10.1016/j.camwa.2021.03.037.

Devries, K., Hall, M., 2018. Comparison of seabed friction formulations in a lumped-mass mooring model. In: ASME 2018 1st International Offshore Wind Technical Conference. http://dx.doi.org/10.1115/IOWTC2018-1099.

Feng, A., Bai, W., You, Y., Chen, Z., Price, W., 2016. A rankine source method solution of a finite depth, wave-body interaction problem. J. Fluids Struct. 62, 14–32. http://dx.doi.org/10.1016/j.jfluidstructs.2016.01.002.

Feng, A., Kang, H., Zhao, B., Jiang, Z., 2020. Two-dimensional numerical modelling of a moored floating body under sloping seabed conditions. J. Mar. Sci. Eng. 8, 389. http://dx.doi.org/10.3390/jmse8060389.

Flexcom, 2021. 3D Seabed profile. https://flexcom.fea.solutions/theory_seabed_3d_profile.html (Accessed May 2022).

Gobat, J., Grosenbaugh, M., 2001. Dynamics in the touchdown region of catenary moorings. Int. J. Offshore Polar Eng. 11.

Hall, M., Goupee, A., 2015. Validation of a lumped-mass mooring line model with DeepCwind semisubmersible model test data. Ocean Eng. 104, 590–603. http://dx.doi.org/10.1016/j.oceaneng.2015.05.035.

Jaiswal, V., Vishnubhotla, S., Cole, S., Gordon, R., Sharma, P., 2016. Impact of bathymetry on the mooring design of an offshore floating unit. In: International Conference on Offshore Mechanics and Arctic Engineering. In: Volume 1: Offshore Technology; Offshore Geotechnics, http://dx.doi.org/10.1115/OMAE2016-54965.

Kaya, H., 2022. Fractal landscape generation with diamond-square algorithm. MATLAB Central File Exchange, https://www.mathworks.com/matlabcentral/fileexchange/44714-fractal-landscape-generation-with-diamond-square-algorithm.

Kelley, C., 2003. Solving nonlinear equations with Newton's method. http://dx.doi.org/10.1137/1.9780898718898.

Lee, D., Schachter, B., 1980. Two algorithms for constructing a delaunay triangulation. Int. J. Comput. Inf. 9, 219–242. http://dx.doi.org/10.1007/BF00977785.

Mahfouz, M., Salari, M., Hernández, S., Vigara, F., Molins, C., Trubat, P., Bredmose, H., Pegalajar-Jurado, A., 2020. COREWIND D1.3: Public design and FAST models of the two 15MW floater-turbine concepts. Tech. Rep., USTUTT, ESTEYCO, UPC, DTU.

Montano, A., Restelli, M., Sacco, R., 2007. Numerical simulation of tethered buoy dynamics using mixed finite elements. Comput. Methods Appl. Mech. Engrg. 196 (41), 4117–4129. http://dx.doi.org/10.1016/j.cma.2007.04.012.

Orazi, L., Reggiani, B., 2020. A novel algorithm for a continuous and fast 3D projection of points on triangulated surfaces for CAM/CAD/CAE applications. J. King Saud Univ. - Comput. Inf. Sci. 9–22. http://dx.doi.org/10.1016/j.jksuci.2020.06.005.

OrcaFlex, 1987-2022. Environment: Seabed data. https://www.orcina.com/webhelp/OrcaFlex/Default.htm (accessed May 2022).

Palm, J., Eskilsson, C., Bergdahl, L., 2017. An hp-adaptive discontinuous Galerkin method for modelling snap loads in mooring cables. Ocean Eng. 144, 266–276. http://dx.doi.org/10.1016/j.oceaneng.2017.08.041.

Palm, J., Paredes, G., Eskilsson, C., Taveira-Pinto, F., Bergdahl, L., 2013. Simulation of mooring cable dynamics using a discontinuous Galerkin method. In: Proceedings of the V International Conference on Computational Methods in Marine Engineering. CIMNE, Hamburg, Germany, 29-31 May, 2013, pp. 455–466.

ProteusDS, 2018. Manual. https://dsaocean.com/downloads/documentation (accessed May 2022).

Rodríguez, A., Armesto, A., Guanche, R., Barrera, C., Vidal, C., 2020. Simulation of marine towing cable dynamics using a finite elements method. J. Mar. Sci. Eng. 82, http://dx.doi.org/10.3390/jmse8020140.

Rolfsen, J., Haugen, S., Een, V., Thorsen, H., Seljelid, J., Steiro, T., Vinnem, E., Antonsen, S., 2013. Causal relationships and measures associated with structural and maritime incidents on the norwegian continental shelf. Petrol. Saf. Authority Norway's Tech. Rep..

Thomsen, J.B., Eskilsson, C., Ferri, F., 2017. Assessment of Available Numerical Tools for Dynamic Mooring Analysis: WP1.2 & M1. DCE Technical reports No. 220, Department of Civil Engineering, Aalborg University.

Trubat, P., Molins, C., Gironella, X., 2020. Wave hydrodynamic forces over mooring lines on floating offshore wind turbines. Ocean Eng. 195, 106730. http://dx.doi.org/10.1016/j.oceaneng.2019.106730.